

Photocatalytic Degradation of Diuron: Experimental Analyses and Simulation of HO[•] Radical Attacks by Density Functional Theory Calculations

Marion Carrier,^{*,†} Chantal Guillard,^{*,†} Michèle Besson,[†] Claire Bordes,[‡] and Henry Chermette[‡]

Université de Lyon, Université Lyon 1, CNRS-UMR 5256, IRCELYON, Institut de recherches sur la catalyse et l'environnement de Lyon, 2 avenue Albert Einstein, F-69626 Villeurbanne Cedex, France, and Université de Lyon, Université Lyon 1, CNRS-UMR 5180 Sciences Analytiques Bâtiment ESCPE, rue Victor Grignard F-69622 Villeurbanne Cedex, France

Received: November 18, 2008; Revised Manuscript Received: April 3, 2009

The photocatalytic oxidation of diuron has been performed in presence of TiO₂ suspensions. To better understand the mechanistic details of the hydroxyl radical attack on diuron, computational methods were carried out. The combination of experimental and computational methods has been employed to establish the main degradation pathways of diuron. After identification of the majority of first byproduct, the experimental study underlined that substitution of chlorines and hydroxylation by hydroxyl radicals are the main diuron degradation pathways, in agreement with MOPAC and DFT simulations carried out in the gas phase. In addition, these calculations revealed that the aromatic ring attack is led by a HO[•] addition and not a hydrogen abstraction and the main first byproduct, monochlorohydroxylated compounds, are obtained by concerted reactions.

1. Introduction

Various pesticides are widely used in agricultural areas. Their extensive use causes a pollution of soils and aquatic systems by soil leaching. Among these chemicals, diuron [3-(3,4-dichlorophenyl)-1,1-dimethylurea] (Figure 1), a commonly used herbicide is considered as highly toxic and persistent (half-life in soil over 370 days).¹

Efficient elimination of this herbicide from unused treatment aqueous solutions may be performed by an advanced oxidation process (AOP), the photocatalysis. Upon adsorption of photons with energy larger than the bandgap of TiO₂ (wavelength lower than 384 nm), electrons in the valence band are excited to the conduction band, generating an electron–hole (e⁻/h⁺) pair. These pairs are able to initiate oxidation and reduction reactions at the TiO₂ surface. The positive holes can oxidize the organic molecules adsorbed at the surface, through the formation of HO[•] radicals or directly by the hole. On the other hand, the photogenerated electron can produce radical species such as superoxide O₂^{•-} and hydroperoxide HO₂^{•-}. All these radicals initially oxidize the substrate into intermediates which subsequently undergo a complete mineralization.

Many works concerning phenylurea products have been performed using TiO₂ photocatalysis in solution: Monuron,² fenuron,^{3,4} metoxuron,³ isoproturon,^{5,6} chlortoluron,⁷ metobromuron.^{8,9} Concerning the diuron molecule, the authors identified different intermediates: 3-(3,4-dichlorophenyl)-6-hydroxyl-1,1-dimethylurea,^{10,11} 3-(3,4-dichlorophenyl)-1-(hydroxymethyl)-1-methylurea,^{11,12} 3-(3-hydroxy-4-chlorophenyl)-1,1-dimethylurea,^{10,11} 3-(3-chloro-4-hydroxyphenyl)-1,1-dimethylurea,^{10,11} 3-(3,4-dichlorophenyl)-1-methylurea,^{10–12} (3,4-dichlorophenyl)urea,¹² 3-(3,4-dichlorophenyl)-1-methyl-1-formylurea,^{10–12} 3-(3,4-di-

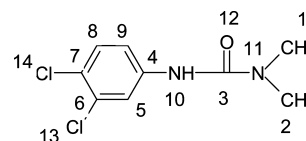


Figure 1. Diuron molecule.

chlorophenyl)-1-methyl-1-carboxylurea,¹¹ 3-(4-chlorophenyl)-1,1-dimethylurea,¹¹ 3-(3,4-dichlorohydroxyphenyl)-1-(hydroxymethyl)-1-methylurea,¹¹ 3-(3-chloro-4-dihydroxyphenyl)-1,1-dimethylurea,¹¹ 3-(3,4-dichlorohydroxyphenyl)-1-methyl-1-formylurea,¹¹ 3-(3,4-dichlorohydroxyphenyl)-1-methylurea,¹⁰ 3-(3,4-dichlorophenyl)-1-(hydroxymethyl)urea,^{11,12} 3-(3,4-dichlorophenyl)-1-formylurea,¹² 3-(3-hydroxy-4-chlorophenyl)-1-methylurea,¹⁰ (3,4-dichlorophenyl)isocyanate,¹¹ 3,4-dichloroaniline,¹¹ hydroquinone,¹¹ phenylisocyanate,¹¹ and aniline.¹⁰ The main degradation pathways seemed to be cycle and methyl hydroxylations by attack of HO[•], loss of one of the methyl groups, and dehalogenation.

Different mechanisms were proposed. In this way, some authors^{8,9,11} illustrated the aromatic ring hydroxylation by hydroxyl radical addition or hole and water attacks, allowing the formation of ortho and para hydroxylated compounds. Others^{3,13} insisted on the role of electron-donor group (EDG) of urea group to explain hydroxyl radical attacks on ortho and para positions. Moreover, Palmisano et al.^{14,15} showed that the primary photocatalytic oxidation of aromatic compounds containing an EDG mainly gives rise to ortho and para monohydroxy derivatives, whereas in the presence of an electron-withdrawing group (EWG) all the monohydroxy derivatives are obtained.^{16,17}

Even if these studies improve the understanding of the primary photocatalytic oxidation of aromatic compounds, the details of reaction mechanisms are incomplete and it becomes difficult to discern the reactivity of the hydroxyl radical itself. Indeed, radicals are species with a single, unpaired electron

* Corresponding authors. Fax: +33 047 2445 399. E-mail: M.C., carrier@sun.ac.za; C.G., chantal.guillard@ircelyon.univ-lyon1.fr.

[†] CNRS-UMR 5256.

[‡] CNRS-UMR 5180.

whose state involves a singly occupied molecular orbital (SOMO) in molecular orbital theory. A radical can exhibit both electrophilic and nucleophilic behaviors.

Using the CAChe software¹⁸ and the semiempirical MOPAC package,¹⁹ Horikoshi showed that the adsorption of amino acids onto the TiO₂ particle surface depends on the point charges of the pollutant. Moreover, primary attack of the amino acids by the HO° radical is correlated with the frontier electron densities.^{20–23} Horikoshi et al. considered globally that the photooxidation mineralization is indicated by the surface-bound HO° radical species and that these species are highly electrophilic, so that the primary position(s) for HO° radical attack are expected to be located on those atoms with the largest electron density. Such calculations were applied to the photocatalytic degradation of imazapyr,²⁴ determining two major pathways by LC–MS: decarboxylation and hydroxylation.

In a different approach, previous works on the determination of byproduct combining experimental results and ab initio calculations were realized by Peller et al.²⁵ They explained the origin of the observed selectivity in the photooxidation of (2,4-dichlorophenoxy)acetic acid (2,4-D). They determined gas-phase and water-continuum model energies of the various hydroxyl radical attacks on 2,4-D using density functional theory (DFT) calculations with the popular B3LYP functional²⁶ coupled to the 631G* basis set.²⁷ Their calculations indicated that all the hydroxyl radical additions to the aromatic ring of 2,4-D were highly exothermic reactions that are energetically favorable. Ipso attacks on C₁, C₂, and C₄ of the aromatic ring were preferred over attacks at the unsubstituted positions of the ring by a significant margin. That was consistent with the observation that no hydroxylated 2,4-D intermediates were identified in the experimental work.

In the present research, the photocatalytic degradation pathways of diuron are studied by using a combination of experimental and computational investigations. In a first part, we study the photocatalytic degradation of diuron by quantitative measurements of the concentration of identified products, total organic carbon (TOC) mineralization and heteroatom mineralization. The identification by LC–MS of some primary products of oxidation resulting from the photocatalytic degradation of diuron allowed us to propose reaction pathways.

The second part consists in understanding the hydroxyl radical attacks onto different atoms of the diuron molecule using DFT theory. For that purpose, the following strategy was used:

- (1) Geometry optimization of diuron.
- (2) Simulation of HO° attacks (substitution or addition) on the different atoms of the aromatic cycle and of the exocyclic chain of diuron.
- (3) Determination of energy barriers.
- (4) Determination of the energy of each product for the energy barrierless paths.

These different steps have permitted the determination of the main pathways of diuron degradation, which were in agreement with experiments and results.

2. Experimental Part

Chemicals and Reagents. Diuron was supplied by Aldrich. (3,4-Dichlorophenyl)isocyanate, 3-(3-chlorophenyl)-1,1-dimethylurea, 1-(3,4-dichlorophenyl)urea, 1-(3,4-dichlorophenyl)-3-methylurea, 3-(3,4-dichlorophenyl)-1-formyl-1-methylurea were obtained from Sigma-Aldrich.

The photocatalyst used in our study was TiO₂ Degussa P-25. TiO₂ exists in two main crystallographic forms, 80% anatase and 20% rutile. Anatase has always been found to be photo-

catalytically more active than rutile.^{28,29} The BET surface area is ca. 50 m² g⁻¹.

Reactor and Light Source. The batch photoreactor was a cylindrical flask made of Pyrex of ca. 100 mL with a bottom optical window of ca. 4 cm diameter which was open to the air. UV irradiation was provided by a high pressure mercury lamp and was filtered by a circulating-water cell equipped with a 340 nm cutoff filter (Corning 0.52). The water cell was used to remove IR radiation, thus preventing any heating of the suspension.

The radiant flux was measured with a radiometer detector model VLX 3W Bioblock scientific. The response bandwidth of the radiometer was centered on 365 nm. The result gave approximately 6 mW cm⁻² at this wavelength, corresponding to a total of UV equal to 14 mW cm⁻².

Photocatalytic Degradation Procedure. The photocatalytic test was performed at room temperature (20 °C). TiO₂ (12 mg) were added, under stirring, to 20 mL of a 40 ppm (180 μmol L⁻¹) aqueous solution of the pesticide. The reaction medium was maintained in the dark for 30 min to reach the adsorption equilibrium. At time $t = 0$, the photoreactor was irradiated. Samples from the suspension (0.5 mL) were taken at regular time intervals for analysis. An amount of 12 mg of TiO₂ was chosen to allow a complete adsorption of the UV-light entering the photoreactor as previously determined.³⁰

Analysis of Reaction Products. Aliquots of solution taken after different times of irradiation were filtered through 0.45 μm PVDF Hydrophilic filters (Millipore) to remove TiO₂ particles before analysis.

The HPLC–UV analyses were performed using a Shimadzu system with a diode array detector and on a 125 mm by a 4 mm C18 reverse-phase column (Uptisphere HDO, Interchim), regulated at 303 K. The mobile phase was methanol with addition of phosphoric acid aqueous buffer adjusted to pH = 2.8 at a ratio 50:50. The eluent flow rate was fixed (0.2 mL min⁻¹). The detection wavelength was set at 254 nm.

Identification of degradation intermediates was determined using LC–MS (electrospray ionization) in positive and negative modes with a (50) (methanol; water acidified with formic acid) mobile phase equipped with the C18 reverse-phase column. To improve results in LC–MS, a preconcentration of the samples was performed on OASIS HLB (hydrophilic balanced copolymer) cartridges. Intermediates adsorbed in the solid phase of cartridge from 20 mL of solution were extracted by 500 μL of methanol.

Identification and quantification of ionic intermediates were performed by an ion chromatograph (IC, Dionex DX-120) equipped with a Dionex Ion Pac CS 12A column (4 × 250 mm) for cations, a Dionex IonPac AS14A (4 × 250 mm) for anions and a conductivity detector. The eluent was 22 mM sulfuric acid for cations or 8 mM Na₂CO₃/1 mM NaHCO₃ for anions. The eluent flow rate was fixed (1 mL min⁻¹).

To complete the carbon balance, TOC was measured with a Shimadzu 5050A TOC analyzer, which employs high temperature combustion oxidation coupled with a non dispersive infrared detection.

Computer Simulations. The experimental work of diuron pathway degradation was completed by computational studies using density functional theory (DFT) within the Kohn–Sham approach. Kohn–Sham DFT is becoming an important first-principles computational method to predict chemical properties accurately and optimize molecule geometry and search energy paths from reactants, via transition states, to final products. For the purpose, the Amsterdam Density Functional (ADF) soft-

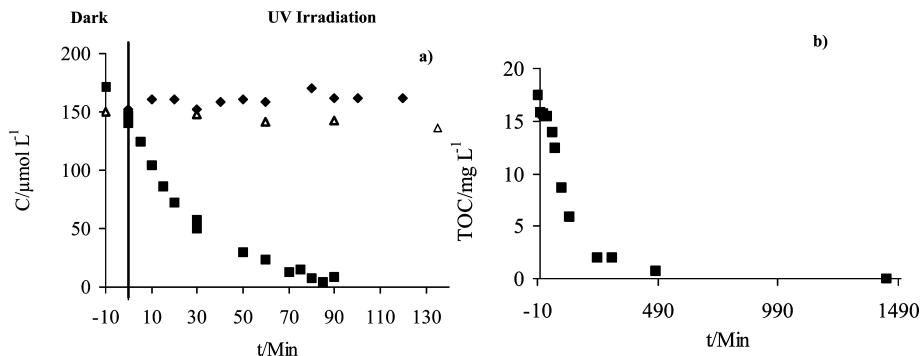


Figure 2. (a) (◆) Adsorption, (△) photolysis, and (■) photocatalysis of diuron ($180 \mu\text{mol L}^{-1}$). (b) TOC evolution during photocatalytic treatment of diuron.

ware³¹ (ADF2005 and 2006 releases) has been used. These calculations were performed using a double ζ basis set augmented by a polarization function (DZP) for the whole reaction path. Small frozen core approximation has been used for 1s orbital shells. This basis set of medium quality has been retained to save computational time with respect to larger basis sets like TZP, which would have led to more accurate energies at the expense of substantially larger computation demand. Geometry optimizations were carried out without any symmetry restriction. In all cases, the nature of the extrema (minimum and transition state structures) was verified through frequency calculations. The exchange-correlation functional adopted was the PBE,³² which is considered as one of the most accurate functionals belonging to the generalized-gradient-approximation (GGA) family.³³ However, it is known that energy barriers are often underestimated with such approach if compared to those obtained using hybrid functional, more computationally demanding.³⁴

3. Results and Discussion

Photocatalytic Degradation of Diuron. Figure 2 shows the concentration of diuron during the blank experiment and the photocatalytic treatment, with the evolution of TOC as a function of irradiation time.

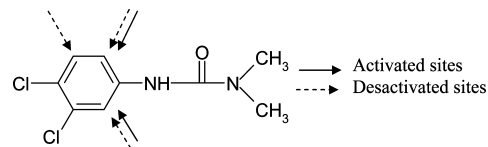
Under only the UV radiation ($\lambda = 365 \text{ nm}$), in the absence of TiO_2 , the disappearance of diuron was negligible. In contact with titanium oxide in the dark, a concentration of $20 \mu\text{mol L}^{-1}$ of diuron was adsorbed at equilibrium, which corresponds to a low adsorption of $2 \times 10^{19} \text{ molecule g}^{-1}$ ($4 \times 10^{17} \text{ molecule m}^{-2}$), that is, a coverage of less than 10% of HO° present on the TiO_2 surface ($5 \times 10^{18} \text{ molecule m}^{-2}$).³⁵ Irradiating the suspension led to the total disappearance of diuron within 90 min (Figure 2a). Mineralization was a longer process, and the total mineralization, followed by measuring the TOC disappearance in the filtered solution, was only complete after a 540 min treatment (Figure 2b).

Identification of Aromatic Byproduct by LC-MS. The different times necessary for total diuron disappearance and total mineralization reflect the presence of several intermediates during the oxidation of diuron. The reaction was stopped at three different times: 5 min, 20 min, and 1 h for analysis of the samples. After filtration, the samples were preconcentrated on a cartridge to concentrate the byproduct and to improve results. The chromatogram after 1 h of photocatalytic degradation corresponding to 86% of diuron conversion is presented in Figure 3. Several transformation products were detected. The main intermediate products were identified by LC-MS and are listed in Table 1.

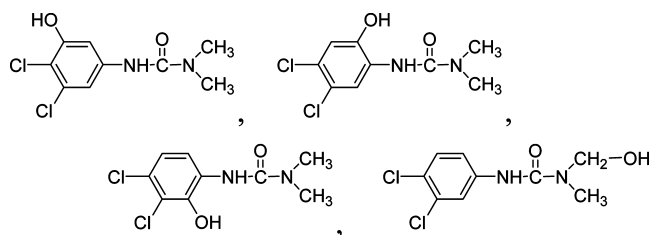
The molecular mass of each product was confirmed by its detection in negative mode or/and in positive mode ($M + 1$ and $M + 23$) (Table 1). The majority of these products were detected in positive mode, while only two were detected in negative mode. They correspond to the following reactions:

- (i) hydroxylation occurring on the aromatic ring or/and the two methyl groups (compounds C, D, E, F).
- (ii) dihydroxylation (compounds G, H).
- (iii) dechlorination (compounds M, N).
- (iv) demethylation (compounds B, K).
- (v) condensation (compound L).

The peak corresponding to the O compound with a mass ion of 278 could not be identified properly. As mentioned in the Introduction, some works^{13–17} deal with the influence of the substituent on the selective photocatalytic oxidation of aromatic compounds in aqueous TiO_2 suspensions. In the present case, two chloride atoms, EW groups, and a urea group, ED group, are present in the diuron structure. The active sites are indicated with arrows, considering an electrophilic attack:



Accordingly, positions in ortho of C–N on the aromatic cycle will be preferentially hydroxylated. However, in our case, four isomers of hydroxylated compounds were identified by LC-MS, indicating the hydroxylation of three positions on the aromatic ring and also a hydroxylation on a methyl group of the exocyclic part of the molecule:



However, the formation of the alcohol might be expected to be a minor pathway. Indeed, Song et al.³⁶ showed that many steps were necessary to produce an alcohol or/and an aldehyde. First a hydrogen abstraction and an oxygen attack lead to a peroxy radical. This radical is relatively unreactive and usually

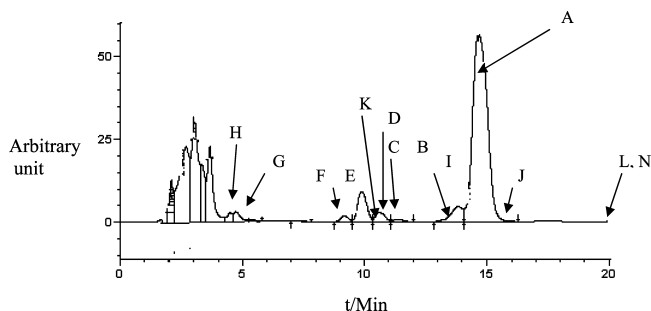


Figure 3. Chromatogram after diuron degradation by photocatalysis (86% diuron conversion).

decays via biomolecular self-termination reactions to form an intermediate tetroxide specie that then undergoes unimolecular decomposition. Then the formation of an aldehyde or/and an alcohol could be possible.

The molecular mass equal to $m/z = 279$ suggests that one nitrogen atom has been lost.

Hence, the identified intermediate products confirm the presence of two main pathways for diuron degradation: deha-

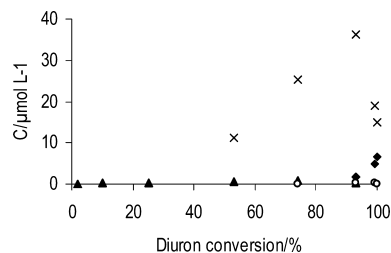


Figure 4. Evolution of carboxylic acids during diuron conversion by photocatalysis: (x) oxalic acid; (▲) maleic acid; (◆) acetic acid; (○) formic acid.

logenation and hydroxylation on the aromatic ring (compounds C, D, E, F, G, H, M, N).

Aliphatic Organic Byproduct: Carboxylic Acids. The evolutions of maleic, oxalic, acetic, and formic acids were followed during the photocatalytic degradation. Oxalic acid gave the most important concentration. The production of these acids occurred after a significant conversion of diuron (Figure 4). In accordance with the chemical structure of diuron, the only way to obtain these acids is a ring-opening by further oxidations of the intermediary compounds. The absence of formic acid at the

TABLE 1: Structure of Diuron and Photoproducts Identified by LC–MS with Electrospray (ES)

ES positive $m/z = M + 1$	ES positive $m/z = M + 23$	ES negative $m/z = M - 1$	Isomer number (Degradatio n time)	Retention time (min) (Figure 3)	Structure	Molecular mass
233/235/237	255/257/259	231/233/235	1(5 min) 1(20 min) 1(1 h)	A		232
249/251/253	271/273/275	247/249/251	4(5 min) 3(20 min) 2(1 h)	C D E F		248
219/221/223	249/251/253		1(5 min) 1(20 min)	B		218
265/267/269			1(5 min) 2(20 min) 2(1 h)	G H		264
215/217	237/239	213/215	2(5 min) 2(20 min) 1(1 h)	M N		214
					or 	
263/265/267	285	261/263/265	2(20 min) 2(1 h)	I J		262
		203/205/207	1(20 min) 1(1 h)	K		204
		245/247/249	1(20 min) 1(1 h)	L		246
280	302	278	1(1 h)	O	?	279

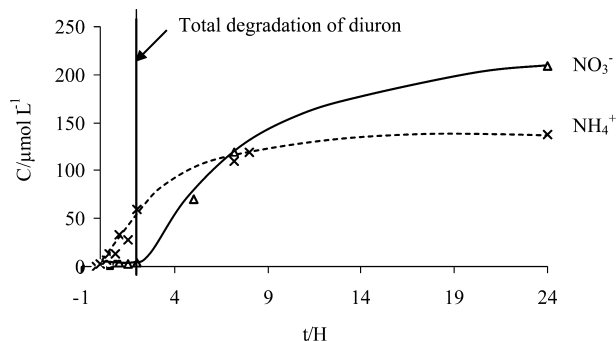


Figure 5. Nitrate ions (Δ) and ammonium (\times) evolution during the photocatalytic process.

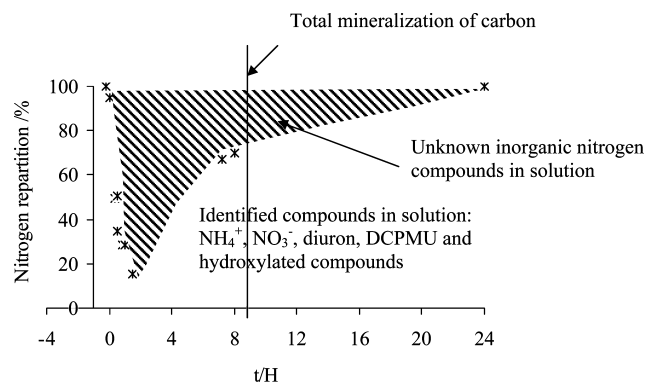


Figure 6. Nitrogen balance during the photocatalytic degradation of diuron.

beginning of diuron degradation and the formation of demethylated compounds indicate that a part of methyl groups would be oxidized into COOH and further onto CO_2 and H_2O .

Mineralization of Heteroatoms. The formation of inorganic ions (NO_3^- , NH_4^+ , Cl^-) was measured in the course of the photocatalytic reaction. The nitrogen mineralization was followed by measuring nitrates and ammonium ion concentrations (Figure 5). The amount of nitrogen remaining in the solution was evaluated from the quantified concentration of identified nitrogen compounds in solution (A, B, NH_4^+ , and NO_3^-). Figure 6 gives the percentage of nitrogen analyzed as a function of reaction time. The difference compared to the total theoretical concentration indicates the amount of unidentified nitrogen compounds.

After an irradiation time of 24 h, all nitrogen initially present in diuron was converted into ammonium and nitrate ions, 40% and 60%, respectively (Figure 5). The formation of nitrates occurred only after 5 h, indicating that nitrate ions are not the primary oxidation byproduct. Moreover, after 9 h of irradiation, the TOC conversion was almost complete while the inorganic nitrogen mass balance was still lower than stoichiometry. The concentration of NO_3^- continued to increase to finally reach stoichiometry after 24 h. Other inorganic nitrogen containing compounds such as hydroxylamine^{37–39} could be present in the solution. Indeed, Nohara et al. has also reported that nitrate ions were most likely generated through hydroxylamine intermediates in the photocatalytic oxidation of nitrogenous compounds.⁴⁰ This observation could explain the increase in nitrate concentration after 9 h without any decrease of ammonium concentration. Thus the nitrate ions would be not produced by the oxidation of the ammonium but directly from an inorganic nitrogen group.

The nitrogen atom contained in amino groups is converted into either ammonium or nitrate ions (Figure 5). Various authors suggested that the degradation pathway of nitrogen does depend

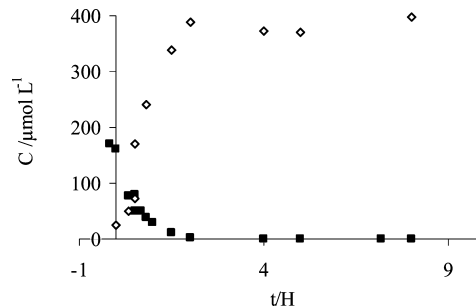


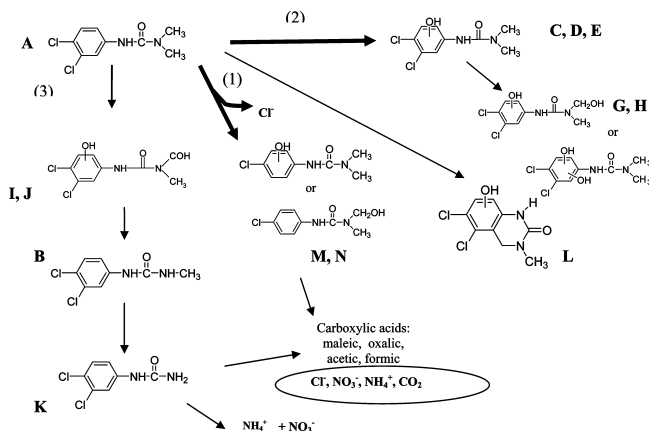
Figure 7. Evolutions of chloride ions (\diamond) during the photocatalytic degradation of diuron (\blacksquare).

not only on its electronic density^{41–43} but also on the initial oxidation state of neighboring carbons.^{40,43}

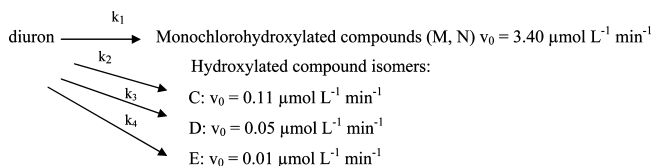
The release of chloride ions into the solution shown in Figure 7 was more rapid than the formations of ammonium and nitrate ions and carboxylic acid, indicating that dechlorination of the aromatic ring of diuron occurs mainly before demethylation and ring-opening. The total chlorine mineralization was reached within 2 h (Figure 7). This result suggests that the initial degradation pathway of diuron is mainly a dechlorination.

Conclusion on Experimental Part. The main photocatalytic degradation pathways of diuron are (1) dehalogenation of the aromatic ring, (2) hydroxylation of the aromatic ring and of the side chain, and (3) demethylation.

The following scheme summarizes all identified products analyzed during the photocatalytic degradation of diuron:



The initial rates of formation of the different hydroxylated compounds obtained from concentration curves as a function of time and the initial rate of release of chloride ions (Figure 7) during the photocatalytic degradation of diuron allow the quantification of the importance of each degradation pathway:



$$\frac{d[\text{diuron}]}{dt} = -k_1[\text{diuron}] - k_2[\text{diuron}] - k_3[\text{diuron}] - k_4[\text{diuron}] = -(k_1 + k_2 + k_3 + k_4)[\text{diuron}]$$

$$\frac{d[\text{diuron}]}{[\text{diuron}]} = -(k_1 + k_2 + k_3 + k_4) dt$$

$$\ln\left(\frac{[\text{diuron}]}{[\text{diuron}]_0}\right) = -(k_1 + k_2 + k_3 + k_4) t$$

$$[\text{diuron}] = [\text{diuron}]_0 \exp(-(k_1 + k_2 + k_3 + k_4) t)$$

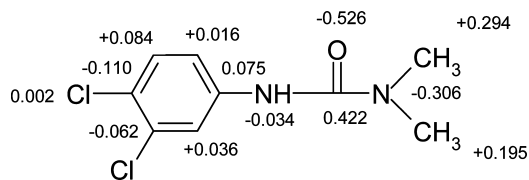


Figure 8. Point charge values determined by MOPAC calculations.

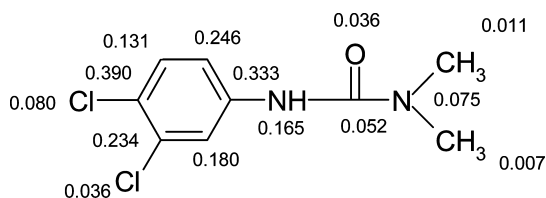


Figure 9. MOPAC results about “radical frontier density” calculation.

The sum of all initial rates of formation, equal to $3.6 \mu\text{mol L}^{-1} \text{min}^{-1}$, is very close to the degradation rate of diuron $3.8 \mu\text{mol L}^{-1} \text{min}^{-1}$, suggesting that the main degradation pathways were identified. But the details of the reaction mechanisms are incomplete, and it becomes difficult to discern the reactivity of the hydroxyl radical itself. Further analysis of the reaction pathway was therefore pursued by using computational methods.

Molecular Modeling Results. LC–MS analysis allowed the identification of some primary intermediate products, among which four are isomers of monohydroxylated compounds. We tried to determine where the main probable attacks of HO° are. We used two calculation methods: MOPAC and DFT. We choose the DFT approach because of its reliability for general chemical reaction modeling, compared to semiempirical methods like those available in the MOPAC package, and its reasonable computational cost with respect to that necessary in post-Hartree–Fock calculations. Indeed, we were aware of the weakness of DFT method for accurate descriptions of radicals, but whereas the Hartree–Fock method would have led to unrealistic modeling, post-Hartree–Fock methods would just require a tremendous computational effort not compatible with the large number of products and reaction paths involved in this study. With the DFT method, and a GGA type of exchange–correlation functional, at least qualitative and relative trustable energies can be expected to be obtained.

MOPAC Calculations. Some calculations were carried out using molecular orbital methods to assess the point charges and the frontier electron density on each atom of diuron. Determining which atom(s) carries the largest negative point charge provides clues as to the direction of approach of diuron and determines ultimate points of adsorption of diuron onto the positively charged surface in acidic aqueous media (pH below 6.3).

The point charge values are presented in Figure 8. Let us recall that these point charges are nothing else than Mulliken charges as deduced from the expansion coefficients of the whole set of molecular orbitals calculated at the semiempirical level. Moreover, hydrogen charges are often set to zero and reported on the atom linked to them.

As expected, the oxygen atom of the carbonyl function is the most negatively charged, it is inferred to be the major point of contact between the positively charged TiO_2 surface and the diuron.

The atomic positions for attack of diuron by HO° radicals can be predicted from the calculated frontier electron densities. They are reported in Figure 9. The values for hydrogen atoms, negligible, are omitted for the sake of clarity.

TABLE 2: Mulliken Charge Calculated through the COSMO Model

atom	Mulliken charge in vacuum	Mulliken charge in model solvent
C ₁	0.252	0.312
C ₂	0.310	0.328
C ₃	0.863	0.853
C ₄	0.178	0.135
C ₅	0.226	0.199
C ₆	-0.234	-0.218
C ₇	-0.247	-0.243
C ₈	0.145	0.182
C ₉	0.005	0.065
N ₁₀	-0.351	-0.273
N ₁₁	-0.621	-0.615
O ₁₂	-0.649	-0.750
Cl ₁₃	0.065	0.002
Cl ₁₄	0.057	-0.001

These numbers are not densities but charges computed within the Cache software¹⁸ through a weighted combination of Mulliken charges of the frontier orbitals, which are supposed to be the most involved in the reactivity of the molecule.

The data show that the carbon atom C₇ is the richest frontier electron density position leading to the loss of chlorine atom. In this regard, the case of HO° attacks on diuron is expected to be in the order C₇ > C₄ > C₉ > C₆ > C₅ > N₁₀ > C₈.

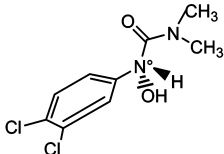
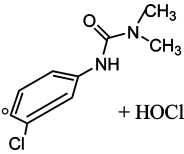
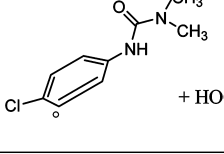
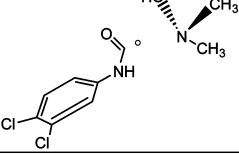
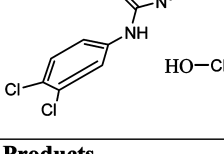
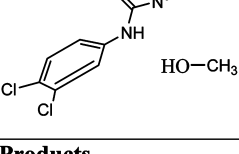
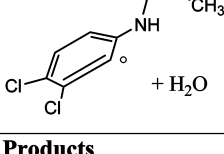
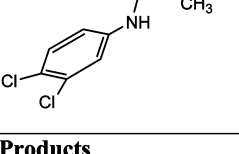
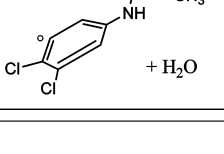
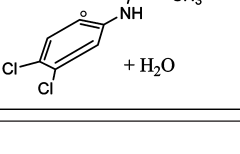
DFT Simulations of HO° Attacks onto Diuron. In the initial hydroxyl radical attack on diuron, energies of reactants and products were established only in gas phase. According to the computed bond data energies of optimized structures of diuron and the HO° radical, -13276 and -670 kJ mol^{-1} , respectively, formation energies as well as barrier energies have been calculated and reported in Tables 3, 4 and 5. Let us recall that the so-called bond energies delivered by ADF software are formation molecular energies with respect to electronic energies of “spherical” atoms, and which cannot be compared to total energies delivered by other softwares. This point is, however, of no importance for the reaction or barrier energies calculations, which are what we are interested in. Mulliken charges are reported in Table 2 and have been calculated through calculations from diuron in a vacuum and in model solvent through the COSMO model.⁴⁴ The last ones take into account the polarity of the solvent, which enhances the polarization of the molecule and, accordingly, the point charges. The values, however, show similar trends among the different parts of the molecule.

Table 3 summarizes the computed barrier energies necessary to attack each atom of the diuron molecule for unfavored transitions. The results of these calculations suggest that some reactions require an excessive amount of energy to be possible. With low barrier energy, HO° attacks hydrogens on the C₅, C₈, and C₉ carbons and C₃ carbon are easier than attacks on the C₁ and C₂ carbons, N₁₁ and N₁₂ nitrogen atoms, and Cl₁₄ and Cl₁₃ chlorine atoms (Table 3).

Concerning energetically favorable reactions (Table 4), we observed barrierless HO° additions on each carbon atom of the aromatic cycle: onto C₆ and C₇ carbons with loss of Cl and onto C₄, C₈, and C₅ and C₉ carbons. On the other hand, hydrogen abstractions onto one methyl group and onto the N₁₀ nitrogen atom localized on the aliphatic chain are favored (Table 4). It is interesting to note that the loss of a chlorine atom leads to non radical products, in contrast to the others attacks.

From the first results, the formation energies of each compound and radical are calculated, and therefore a list of

TABLE 3: Hydroxyl Radical Attacks onto Unfavored Sites (Energy Barriers in kJ mol⁻¹)

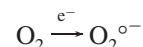
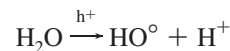
Attack on N₁₀ 182	Products 	Attack on Cl₁₄ 178	Products  + HOCl
Attack on Cl₁₃ 166	Products  + HOCl	Attack on N₁₁ 149	Products 
Attack on C₁ 136	Products  HO-CH ₃	Attack on C₂ 128	Products  HO-CH ₃
Attack on H₅ 54	Products  + H ₂ O	Attack on C₃ 34	Products 
Attack on H₈ 19	Products  + H ₂ O	Attack on H₉ 15	Products  + H ₂ O

relative expected formation of compounds is established (Table 4). Attacks on C₆, and on C₇ are preferred to the unsubstituted positions of the ring by a significant margin. This is consistent with the observation that two monochlorinated and hydroxylated compounds were identified in the experimental work. Attacks on the unsubstituted positions of the aromatic ring and attacks on C₄ and on the side chain are energetically very close.

Let us underline that the influence of the solvent has not been taken into account in these (gas phase) calculations. Indeed, the presence of solvent will certainly modify the relative energies, through a stabilization mechanism of the formed radical (which can be either the product or the chlorine atom (attacks no. 1 and 2)). In this latter case, it has been estimated through a calculation including one explicit water molecule, located between the Cl atom and the oxygen of the phenol group via hydrogen bonds. The net effect takes into account the formation of two hydrogen bonds, one between the chlorine radical, and one between the water oxygen and the phenol group hydrogen, and the disappearance of the hydrogen bonds between this water molecule and the two Cl atoms of the diuron. A thorough analysis of all the solvation sites, involving three or four explicit water molecules, coupled to a solvent modeling through a continuum, is beyond the scope of this work. Anyway, this crude estimation leads to an increase of the reaction energy by an amount of -81 kJ mol⁻¹.

DFT Simulations of HOO° Attacks. If the positive holes can be trapped by surface hydroxyl groups forming a highly

reactive hydroxyl radical, allowing a rapid reaction with almost all organic molecules and thus initiating its oxidative decomposition, the electrons are typically transferred to dioxygen yielding superoxide radical anion (O₂^{o-}):



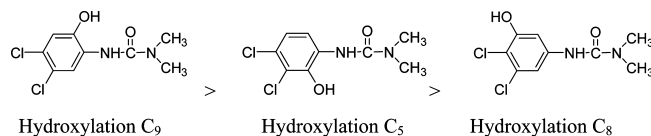
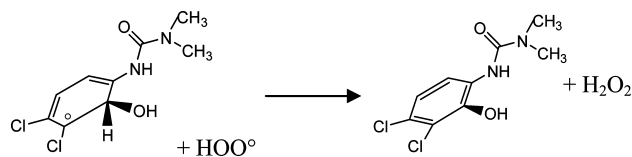
In our pH conditions (pH = 4), the HOO° concentration is higher than the O₂^{o-} concentration:⁴⁵



The dissolved HOO° is an essential reaction component of the photocatalysis participating also in further steps of degradation. It can also repeatedly react with organic radicals originated from the primary HO° attacks leading to other various structures.

First calculations lead to numerous results on intermediate products from aromatic cycle and side-chain attacks whose energy is indicated in Table 4:

• The hydroxylation on each carbon of the aromatic ring, initiated by attacks no. 4, no. 6, no. 7, and no. 8 (Table 4) and followed by HOO° attacks onto C₅, C₈, and C₉ carbons (Table 5), show that C₉ is more easily attacked than C₅ and C₈ according to electronic effects of the urea group and chlorine atoms:¹³



The apparition order for hydroxylated compounds obtained from calculations is the following (Table 5):

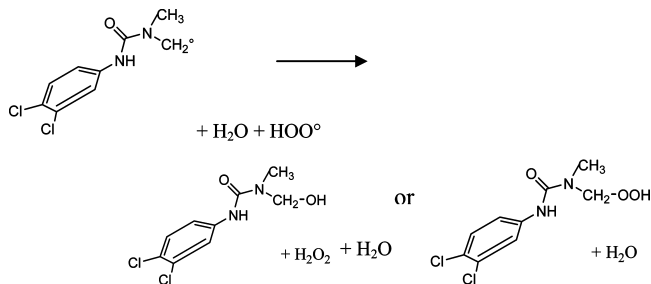
• The HOO^\bullet attack on C_4 leads to a molecule reorganization with the formation of an isocyanate derivative which would be hydrolyzed in our conditions into an amine compound (Figure 10)⁴⁶ and a hydroxylated compound with a peroxy group on C_5 carbon:

LC-MS analysis revealed only the $m/z = 204$ mass, which corresponds to the dichlorophenylurea mass too. A LC-MS/MS analysis would be necessary in this case to clarify the nature of the $m/z = 204$ compound.

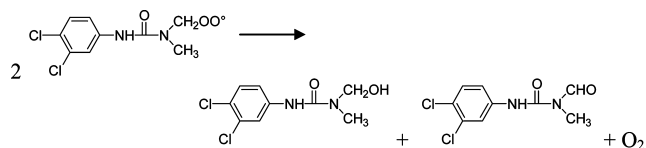
Concerning HOO^\bullet attacks on the side chain of radicals, only one attack of HOO^\bullet (hydrogen of C_1) has led to new products but none of them has been experimentally detected:

TABLE 4: Barrierless Hydroxyl Radical Attacks and Their Products

Attack on	Products	Formation energy (kJ mol^{-1})
Attack n°1 On C_6		(1) -196 (2) -196
Attack n°2 On C_7		-187
Attack n°3 On H of N_{10}		-136
Attack n°4 On C_9		-117
Attack n°5 On H of C_1 On H of C_2		-107
Attack n°6 On C_5		-102
Attack n°7 On C_4	<p>We can notice C_4 attack leads to the formation of 3 possible hydroxyl radicals on C_4, C_5 and C_9.</p>	(1) -92 (2) -99 (3) -117
Attack n°8 On C_8		-89

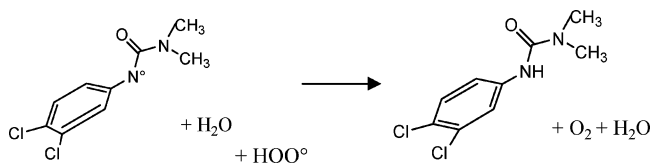


The formation of this peroxide derivative confirms the mechanism proposed by von Sonntag⁴⁷ leading to the (3,4-dichlorophenyl)methylurea (DCPMU) formation:



Within our calculations no DCPMU formation was obtained, suggesting that this product would be not a primary product. According to the literature the formation of DCPMU would result from the hydration of the aldehyde with formic acid formation or/and to the alcohol degradation with loss of formaldehyde.¹² No formic acid formation was measured at the beginning of the photocatalytic reaction during our experiments so that the alcohol formation would be preferred.

• The last HOO° attack on N₁₀ nitrogen atom leads back to the diuron molecule:



These calculations have shown that the main intermediate products from HO° attacks are the hydroxymonochlorinated

TABLE 5: Energy of Reactants and Products from HOO° Attacks on Aromatic Radicals

attack	energy of reactants (kJ mol ⁻¹)	energy of products (kJ mol ⁻¹)
on H of N ₁₀	-15200	-15317
on C ₄	-15156	-15341
on C ₅	-15166	-15431
on C ₈	-15153	-15419
on C ₉	-15181	-15438
on H of C ₁	-15171	-15452

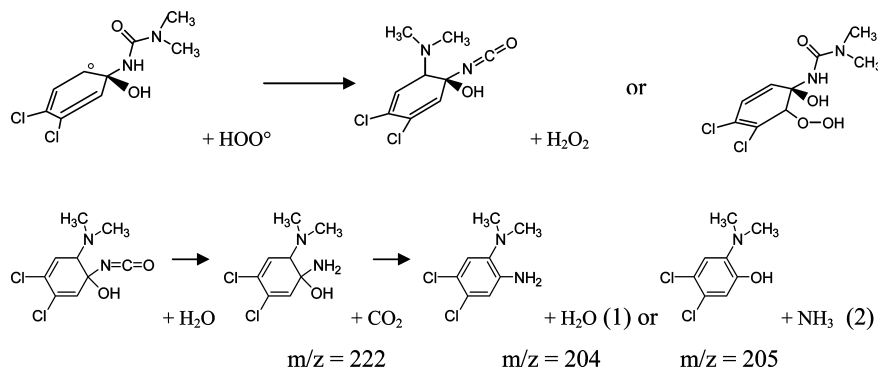


Figure 10. Hydroxylation of the isocyanate derivative.

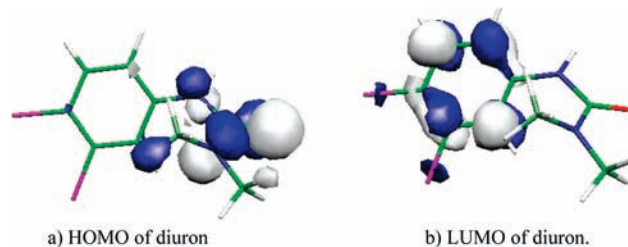


Figure 11. (a) HOMO of diuron. (b) LUMO of diuron.

products via a HO° addition onto carbons in the ipso position of chlorine atoms. According to the DFT calculations, nucleophilic addition on aromatic cycle is preferred to the H-atom abstraction. Hydroxylated products come from radical additions. Therefore one HO° gives one electron to the lowest energy unoccupied molecular orbital (LUMO) of the diuron molecule (Figure 11b), the density of which is mostly developed on the ring. On the other hand, H-atom abstraction will take place only on the side chain where the density of the highest energy occupied molecular orbital (HOMO) is mainly located (Figure 11a).

4. Concluding Remarks

The experimental part has permitted (1) the study of the degradation of the herbicide diuron by photocatalysis in presence of TiO₂ suspensions (the elimination of diuron by this method was demonstrated), (2) the identification of several intermediates and final products with LC-MS, and (3) the conclusion of the chemical mechanism of the diuron oxidation.

The kinetic studies and the analyses of the first intermediate products suggest that substitution of chlorines and hydroxylation by hydroxyl radicals are the main degradation processes of diuron before the opening of the aromatic ring which produced oxalic, maleic, formic, and acetic acids. The study of the evolution of heteroatoms indicates that nitrate ions do not result from ammonium oxidation, as the amount of NH₄⁺ remains constant while the amount of NO₃⁻ was increasing. The nitrogen contained in amino groups is initially converted into NH₄⁺. After the total disappearance of diuron, nitrogen is also converted into NO₃⁻. The mineralization of nitrogen depends on its initial oxidation degree but also on the initial oxidation state of neighboring carbons. The chlorine atoms are completely released as chloride ions.

MOPAC and DFT simulations show that HO° attacks on carbon carrying chlorine atom were the main reactions in agreement with experimental results. Moreover, these two types of theoretical simulations indicate that hydroxylations on C-H of the ring occur in the following order: C₉ > C₅ > C₈ and also suggest that a HO° attack on C₄ is easy.

However, MOPAC calculations show that the HO° attack on C₁ or C₂ is more difficult than attacks on the ring considering only the frontier electron density, whereas DFT calculations show that these reactions have no energy barrier and the formation energies of all monohydroxylated compounds are very close. Our experimental results (LC–MS) show the formation of four monohydroxylated compounds in different proportions. Unfortunately, it has not been possible to identify the position of hydroxylation.

Contrarily to MOPAC, DFT simulations allow us (1) to determine that monochlorohydroxylated compounds are obtained by concerted reactions, (2) to suggest the formation of a new intermediate product from the rearrangement of a radical byproduct resulting itself of the HOO° attack on C₄, (3) to show that HO° attack on cycle was a nucleophilic addition and not a hydrogen abstraction, and (4) to explain that the hydrogen atom abstraction on N₁₀ does not permit hydroxylation.

DFT calculations have been necessary to provide a more detailed discussion of the photooxidation pathways, through an examination of additional data such as the nature of the intermediates formed during HO° attacks. Therefore a more comprehensive view of the complexity of events that take place has been obtained.

Acknowledgment. We extend special thanks to S. Horikoshi for his calculations from MOPAC and K. Rachedi for his participation on ADF calculations. This work was financially supported by Région Rhône-Alpes of France in the Program (2003–2005) entitled: “Evaluation de gains biologique et écologique associés à un réduction d’intrants polluants en milieu aquatique”.

References and Notes

- (1) *The Pesticide Manual*, 11th ed.; Tomlin, C. D. S., Ed.; British Crop Protection and the Royal Society of Chemistry: Farnham, U.K., 1997; pp 443–445.
- (2) Pramauro, E.; Vincenti, M.; Augugliaro, V.; Palmisano, L. *Environ. Sci. Technol.* **1993**, *27*, 1790.
- (3) Amine-Khodja, A.; Boulkamh, A.; Boule, P. *Photochem. Photobiol. Sci.* **2004**, *3*, 145.
- (4) Richard, C.; Bengana, S. *Chemosphere* **1996**, *33*, 635.
- (5) Amorisco, A.; Losito, I.; Palmisano, F.; Zamboni, P. G. *Rapid Commun. Mass Spectrom.* **2005**, *19*, 1507.
- (6) Haque, M. M.; Muneer, M. *J. Environ. Manage.* **2003**, *69*, 169.
- (7) Lhomme, L.; Brosillon, S.; Wolbert, D.; Dussaud, J. *Appl. Catal., B* **2005**, *61*, 227.
- (8) Boulkamh, A.; Sehili, T.; Boule, P. *J. Photochem. Photobiol., A* **2001**, *143*, 191.
- (9) Amine-Khodja, A.; Boulkamh, A.; Richard, C. *Appl. Catal., B* **2005**, *59*, 147.
- (10) Malato, S.; Caceres, J.; Fernandez-Alba, A. R.; Piedra, L.; Hernandez, M. D.; Aguera, A.; Vial, J. *Environ. Sci. Technol.* **2003**, *37*, 2516.
- (11) Canle López, M.; Fernández, M. I.; Rodríguez, S.; Santaballa, J. A.; Steenken, S.; Vulliet, E. *ChemPhysChem* **2005**, *6*, 2064.
- (12) Macounova, K.; Krysova, H.; Ludvik, J.; Jirkovsky, J. *J. Photochem. Photobiol., A* **2003**, *156*, 273.
- (13) Parra, S.; Olivero, J.; Pulgarin, C. *Appl. Catal., B* **2002**, *36*, 75.
- (14) Palmisano, G.; Addamo, M.; Augugliaro, V.; Caronna, T.; Garcia-Lopez, E.; Loddo, V.; Palmisano, L. *Chem. Commun.* **2006**, 1012.

- (15) Palmisano, G.; Addamo, M.; Augugliaro, V.; Caronna, T.; Di Paola, A.; Garcia Lopez, E.; Loddo, V.; Marci, G.; Palmisano, L.; Schiavello, M. *Catal. Today* **2007**, *122*, 118.
- (16) Tuazon, E. C.; Leod, H. M.; Atkinson, R.; Carter, W. P. L. *Environ. Sci. Technol.* **1986**, *20*, 383.
- (17) Pichat, P.; Guillard, C.; Maillard, C.; Amalric, L.; D’Oliveira, J.-C. *Proceedings of the First International Conference on TiO₂: Photocatalytic Purification and Treatment of Water and Air*; Ollis, D. F., Al-Ekabi, H., Eds.; Elsevier: London, 1993; pp 207.
- (18) <http://www.cachesoftware.com/mopac/index.shtml>.
- (19) (a) Stewart, J. J. P. *J. Comput. Chem.* **1989**, *10*, 209. (b) Stewart, J. J. P.; Zheng, J.; Rossi, I.; Hu, W.-P.; Lynch, G. C.; Liu, Y.-P.; Chuang, Y.-Y.; Pu, J.; Li, J.; Cramer, C. J.; Fast, P. L.; Truhlar, D. G. *MOPAC-Version 5.012mm*; University of Minnesota: Minneapolis, MN, 2006.
- (20) Horikoshi, S.; Serpone, N.; Zhao, J.; Hidaka, H. *J. Photochem. Photobiol., A* **1998**, *118*, 123.
- (21) Horikoshi, S.; Watanabe, N.; Mukae, M.; Hidaka, H.; Serpone, N. *New J. Chem.* **2001**, *25*, 999.
- (22) Guillard, C.; Horikoshi, S.; Watanabe, N.; Hidaka, H.; Pichat, P. *J. Photochem. Photobiol. A* **2002**, *149*, 155.
- (23) Almaric, L.; Guillard, C.; Blanc-Brude, E.; Pichat, P. *Water Res.* **1996**, *30*, 1137.
- (24) Carrier, M.; Pérol, N.; Herrmann, J.-M.; Bordes, C.; Horikoshi, S.; Païssé, J. O.; Baudot, R.; Guillard, C. *Appl. Catal., B* **2006**, *65*, 11.
- (25) Peller, J.; Wiest, O.; Kamat, P. V. *J. Phys. Chem. A* **2004**, *108*, 10925.
- (26) (a) Becke, A. D. *J. Chem. Phys.* **1993**, *98*, 5648–5652. (b) Becke, A. D. *Phys. Rev. A* **1988**, *38*, 3098. (c) Lee, C.; Yang, W.; Parr, R. G. *Phys. Rev. B* **1988**, *37*, 785.
- (27) Hehre, W. J.; Radom, L.; Schleyer, P. V. R.; Pople, J. A. *Ab Initio Molecular Orbital Theory*; Wiley: New York, 1986.
- (28) Bielski, B. H. J.; Cabelli, D. E.; Arudi, R. L.; Ross, A. B. *J. Phys. Chem. Ref. Data* **1985**, *14*, 1041.
- (29) Chameides, W. L.; Davis, D. D. *J. Geophys. Res., C* **1982**, *87*, 4863.
- (30) El Madani, M.; Guillard, C.; Pérol, N.; Chovelon, J. M.; El Azzouzi, M.; Zrineh, A.; Herrmann, J. M. *Appl. Catal., B* **2006**, *65*, 70.
- (31) Te Velde, G.; Bickelhaupt, F. M.; Baerends, E. J.; Fonseca Guerra, C.; Van Gisbergen, J. G.; Snijders, S. J. A.; Ziegler, T. *J. Comput. Chem.* **2001**, *22*, 931.
- (32) Baerends, E. J.; et al. *ADF 2006.1, SCM, Theoretical Chemistry*; Vrije Universiteit, Amsterdam: The Netherlands, 2006.
- (33) Perdew, J. P.; Ernzerhof, M.; Burke, K. *J. Chem. Phys.* **1996**, *105*, 9982.
- (34) Chermette, H. *Coord. Chem. Rev.* **1998**, *178–180*, 699.
- (35) Van Damme, H.; Hall, W. K. *J. Am. Chem. Soc.* **1979**, *101*, 4373.
- (36) Song, W.; Cooper, W. J.; Peake, B. M.; Mezyk, S. P.; Nickelsen, M. G.; O’Shea, K. E. *Water Res.*, in press.
- (37) Mozzanega, H.; Herrmann, J.-M.; Pichat, P. *J. Phys. Chem.* **1979**, *83*, 2251.
- (38) Low, G. K.-C.; McEvoy, S. R.; Matthews, R. W. *Environ. Sci. Technol.* **1991**, *25*, 460.
- (39) Oosawa, Y. *J. Phys. Chem.* **1984**, *88*, 3069.
- (40) Nohara, K.; Hidaka, H.; Pelizzetti, E.; Serpone, N. *J. Photochem. Photobiol., A* **1997**, *102*, 265.
- (41) Maurino, V.; Minero, C.; Pelizzetti, E.; Piccinini, P.; Serpone, N.; Hidaka, H. *J. Photochem. Photobiol., A* **1997**, *109*, 171.
- (42) Bui, H. Ph.D. thesis, University of Lyon (FR), 2005.
- (43) Pelizzetti, E.; Calza, P.; Mariella, G.; Maurino, V.; Minero, C.; Maurino, C.; Hidaka, H. *Chem. Commun.* **2004**, 1504.
- (44) (a) Pye, C. C.; Ziegler, T. *Theor. Chem. Acc.* **1999**, *101*, 396. (b) Klamt, A. *J. Phys. Chem.* **1995**, *99*, 2224.
- (45) Bielski, B. H. J.; Cabelli, D. E.; Arudi, R. L.; Ross, A. B. *J. Phys. Chem. Ref. Data* **1985**, *14*, 1041.
- (46) Salvestrini, S.; Di Cerbo, P.; Capasso, S. *Chemosphere* **2002**, *48*, 69.
- (47) von Sonntag, C.; Schuchmann, H.-P. *Angew. Chem., Int. Ed. Engl.* **1991**, *30*, 1229.